Spectrochimica Acta Part B 137 (2017) 28–38

Contents lists available at ScienceDirect

Spectrochimica Acta Part B

journal homepage: www.elsevier.com/locate/sab

Calibration approach for extremely variable laser induced plasmas and a strategy to reduce the matrix effect in general☆

V. Lazic *, A. De Ninno

ENEA (FSN-TECFIS-DIM), Via. E. Fermi 45, 00044 Frascati (RM), Italy

ARTICLE INFO

Article history:
Received 28 February 2017
Received in revised form 31 May 2017
Accepted 9 September 2017
Available online 18 September 2017

Keywords:
Laser induced breakdown spectroscopy LIBS
Plasma
Calibration
Matrix effect
Particles

ABSTRACT

The laser induced plasma spectroscopy was applied on particles attached on substrate represented by a silica wafer covered with a thin oil film. The substrate itself weakly interacts with a ns Nd:YAG laser (1064 nm) while presence of particles strongly enhances the plasma emission, here detected by a compact spectrometer array. Variations of the sample mass from one laser spot to another exceed one order of magnitude, as estimated by on-line photography and the initial image calibration for different sample loadings. Consequently, the spectral lines from particles show extreme intensity fluctuations from one sampling point to another, between the detection threshold and the detector's saturation in some cases. In such conditions the common calibration approach based on the averaged spectra, also when considering ratios of the element lines i.e. concentrations, produces errors too large for measuring the sample compositions. On the other hand, intensities of an analytical and the reference line from single shot spectra are linearly correlated. The corresponding slope depends on the concentration ratio and it is weakly sensitive to fluctuations of the plasma temperature inside the data set. A use of the slopes for constructing the calibration graphs significantly reduces the error bars but it does not eliminate the point scattering caused by the matrix effect, which is also responsible for large differences in the average plasma temperatures among the samples. Well aligned calibration points were obtained after identifying the couples of transitions less sensitive to variations of the plasma temperature, and this was achieved by simple theoretical simulations. Such selection of the analytical lines minimizes the matrix effect, and together with the chosen calibration approach, allows to measure the relative element concentrations even in highly unstable laser induced plasmas.

1. Introduction

Quantitative analysis by laser induced breakdown spectroscopy (LIBS) normally requires an initial calibration with matrix similar samples [1] because the signal depends on physical and chemical properties of material (matrix effect). Accurate LIBS measurements of the element concentrations are difficult to achieve on complex and unknown materials, as it commonly occurs with geological samples [2,3]. For this reason, calibration of the ChemCam LIBS instrument, employed for Mars exploration, involved even 69 different rock types. Nonetheless, in some cases the LIBS measured contents, also of some major elements like silica and iron, differ up to 30% from true values [3]. A significant improvement of the precision might be achieved by normalizing intensities of the analytical lines by the continuum plasma emission, by the integrated plasma intensity or by the line intensity from some major element in sample [4,5]. However, if the laser induced plume has parameters very different from one matrix to another, the calibration graphs remain poor unless the signal is normalized on the plasma temperature [6,7]. A complete correction procedure for calibration in presence of variable plasma parameters from one sample to another is described in [8].

In a large majority of LIBS experiments the calibration needs extended measurements except in case of a very high reproducibility, where a single pulse acquisition might be sufficient [9]. Unstable LIBS signal produces large error bars in calibration graphs due to fluctuations of the plasma parameters from one spectrum to another. In such cases, the precision could be improved by calculating the plasma parameters for each spectrum and correcting the line intensities as mentioned previously. However, this approach is extremely time consuming and difficult to implement on large data sets. Recently, an attempt to correct empirically the line intensities for variations of the plasma temperature has been reported [10]. This correction procedure is based on retrieval of four fitting coefficients from the acquired data set, and it improved linear correlation between the measured line intensity ratios and the certified concentration ratios in samples. Another rapid and easy to

☆ Selected paper from the 9th International Conference on Laser-Induced Breakdown Spectroscopy (LIBS), Chamonix-Mont-Blanc, France, September 12 – September 16 2016.

* Corresponding author.
E-mail address: violeta.lazic@enea.it (V. Lazic).

https://doi.org/10.1016/j.sab.2017.09.001
0584-8547/

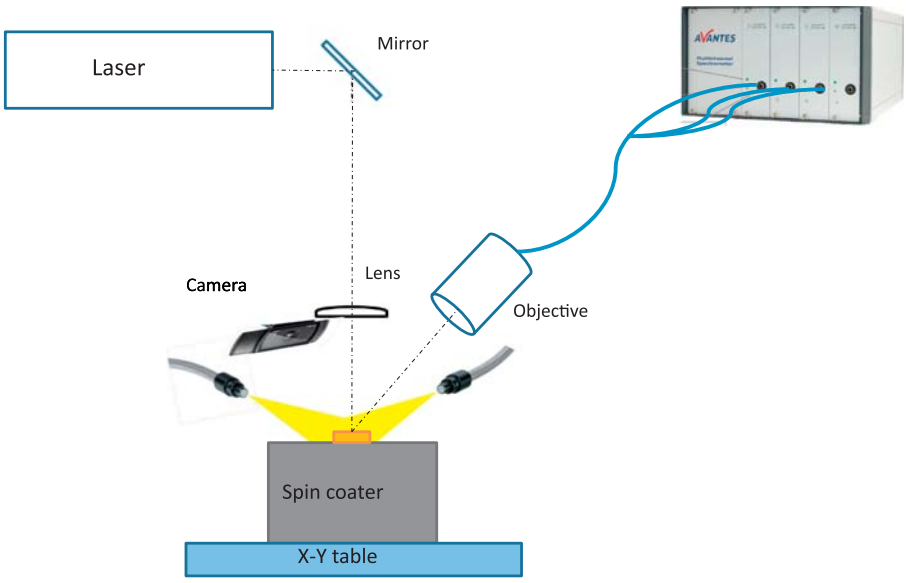

Fig. 1. Experimental layout.

apply procedure for correcting the effects of variable plasma parameters is based on line normalization by the overall plasma intensity, with the coefficients specific for each analytical line [5]. This approach is particularly useful in stratigraphic measurements, and it was successfully applied to determine composition of different layers on ancient ceramics.

Most of the LIBS works report fluctuations of the line intensities inside one order of magnitude except those relative to sampling of floating particles in gases or to the measurements inside liquids. In presence of extremely large plasma intensity fluctuations, averaging of the spectra leads to poor analytical performances. Here, the measurement sensitivity and precision might be drastically improved by applying conditional analysis where only spectra carrying the intense signal are considered [11,12].

LIBS analysis of powders pressed into pellets, like soils or finely grinded plant materials, is well established procedure [8,13–14]. The sampling is performed always on a fresh surface in order to avoid the signal variations due to crater development, and the material must be available in weights of 1 g or higher. A possibility to determine by LIBS the chemical composition of powders in small quantities was first explored by Gornushkin et al. [15]. Different types of particles were attached to a double-sided tape and the signal was averaged over 8–10 laser spots. A good calibration curve was obtained for one Mg I transition after normalizing the measured line intensity on particle density. The latter was estimated from area occupied by the particles and from weight of the deposited material. In this way, the relative error was 10–20%, satisfactory for complex samples like those geological. In [16] comparative LIBS analyses were performed by averaging the spectra over pressed pellets or over particles on a tape. Calibration for measuring Fe and Al content in particles involved $CaCO_3$ and SiO_2 matrixes. The authors observed a reduced matrix effect for particles on tape with respect to the pellets. This was explained by different ablation rates for the two matrixes when pressed into pellets while the corresponding particles on tape were always fully ablated by a laser pulse.

Table 1
Spectrometer's acquisition ranges, here used ranges and the measured linewidths.

Spectrometer No.	Acquisition range (nm)	Used Range (nm)	Linewidth (nm)
1	236.3–406.0	236.3–400.0	0.09
2	398.2–546.2	400.0–546.2	0.10
3	570.0–796.3	570.0–796.3	0.16

LIBS measurements of particles were mainly developed for environmental monitoring, aimed to determine their concentration in air. Indirect analyses of particles deposited on filters by a forced gas flux are more efficient than direct sampling of aerosol [17]. In the first case, after averaging many spectra across the filter, it is possible to retrieve a total mass of some element accumulated over a certain period [17–19]. The typical detection limits are from 0.01 to 0.44 μg/cm^2; the measurement precision also depends on particle size and penetration into the filter [11,17]. Another sample preparation method for trapping and analyzing particles by LIBS was proposed in [20]. Particles were mixed with certified pure oil and then the mixture was spread over pure, polished aluminum. The sampling was performed by scanning the substrate and accumulating the spectra over 200 laser shots. The metallic substrate enhances particle-laser interaction and the estimated plasma temperature reaches 15000 K. Good calibration curves were obtained for Ti diluted in cellulose or alumina powders, but their slopes differed for the two matrixes. The matrix effect was then reduced by normalizing the analytic line on the known material density.

Chemical characterization of particles in small quantities by LIBS has many potential applications, where a suitable sample preparation could also substitute pressing of powders into pellets [13–14]. The final scope of this work was to obtain highly sensitive, quantitative LIBS analyses of unknown particles on substrate. This task is extremely complex due to a variable particle distribution, the interference of a substrate, and the matrix effect. Here we performed the work in different steps:

1) Establishing of a simple sample preparation procedure, which preferably enhances the spectral emission from particles while keeping simultaneously the substrate's interference low.
2) Estimating the changes of particle mass and distribution inside laser spot in order to evaluate the effects on the spectra.
3) Once ascertained that the plasma parameters are highly variable inside the data set for one sample, producing very large errors in calibration graphs, we developed a novel calibration procedure that mitigates this problem.
4) We found that the points in the calibration graphs remain scattered in some cases due to the matrix effect, which causes very different average plasma temperatures among the samples. The final step of our work regards theoretical simulations aimed to select for calibration the line couples less sensitive to the temperature changes.

At the end, we also discuss the advantages of here proposed calibration approach for reducing the matrix effect in LIBS measurements in general.

2. Experimental

The experimental set-up is schematically drawn in Fig. 1. The plasma was generated by an Nd:YAG laser (Quantel, CFR Ultra) emitting 6.5 ns long pulses at 1064 nm; the laser energy was fixed to 130 mJ. The laser was fired manually after repositioning the target. The beam was focused by a quartz lens f = 100 mm perpendicular to a horizontally placed target, mounted on a micrometric X-Y table. The substrate height was slightly above the focal plane and the spot diameter, measured on bare silica wafer, was of 0.42 mm, corresponding to laser fluency of 94 J/cm^2 (14.4 GW/cm^2). The target was shifted for 2 mm between two subsequent samplings; such a distance could be reduced to about 1.2 mm, sufficient to avoid the material removal by the shockwaves generated by the previous laser pulses.

The plasma emission was collected at angle of about 60° from the target plane by an optical system of diameter 25.4 mm and having two quartz lenses with focal lengths of 75 mm and 150 mm, respectively. The light was focused on a 1 m long fiber bundle containing three quartz fibers with diameter 600 μm each, that bring the signal to three compact spectrometers (Avantes AvaSpec-ULS2048L). The spectrometer's full and here used ranges, and the linewidths (instrument broadening) measured by the calibration lamps, are summarized in Table 1.

The chosen substrate consists of silica wafer (P-type Silica, with a 285 nm thick SiO_2 layer, Graphene Supermarket, W-5P-300) covered with a pure reference oil (Base Oil 75, SpexCertPrep). The wafer was cut manually into pieces with maximum dimensions of 15 mm × 15 mm, and glued on an aluminum disk that matches the spin-coater (Laurell Technologies, KL-SCI-20). The oil was delivered in volume of 10 μL by means of an autoclavable pipette (Labgene Scientific), and the support was rotated for 30 s at speed of 40 rpm. During rotation an excess of the liquid detaches from the wafer, leaving an uniform oil layer with the average thickness of about 10 μm. The oil film thickness was estimated for a droplet with volume $V = 0.5$ μL, placed at the wafer's center. After the rotation as above, the area A on the wafer occupied by the oil film was determined from dimensionally calibrated photographs by using ImageJ software (free source). The average oil thickness d on the substrate was then calculated as $d = V/A$.

The samples analyzed (Table 2) were in form of fine powders and include four soil samples and two coal based materials. We also tested Al_2O_3 polishing powder (Union Carbide) with the grain size of 1 μm in order to evaluate contribution from the wafer/oil to the LIBS spectra for different particle quantities inside the focal spot. For depositing the particles we employed an air cleaner brush, commonly used to clean photographic lenses. Particles inside a clean glass dish were collected by the brush and blown on the substrate. For each sample we did measurements along 5 lines with 7 spots each, starting with low particle presence and later blowing more material on the substrate. Furthermore, another 7 or 14 spectra per sample were acquired at random positions, selected due to different particle distribution, as for example: a single grain or a spot only partially covered.

Table 2
Analyzed powder samples, their description and the main constituents (in %).

Sample	Type	Silicon	Aluminum	Calcium	Carbon
NIST 2709	Agricultural soil	29.7	7.50	1.89	1.2[a]
NIST 2710	Highly contaminated soil	29.0	6.44	1.25	3[a]
NIST 2711	Moderately contaminated soil	30.4	6.53	2.88	2[a]
ISE 992	Sand clay	33.5	3.65	2.94	3.9
SRM 1632a	Coal bituminous	5.9	2.95	0.241	64.4
SRM 1633b	Coal fly ash	23.0	15.0	1.51	–

[a] Consensus values.

Table 3
List of the measured lines, the corresponding excitation energies E_k and the transition probabilities g_kA_k according to the NIST database; in the last column the first ionization energies E_∞(eV) are also specified.

No.	Species	λ (nm)	E_k (eV)	A_kg_k	E_∞(eV)
1	Al I	309.3	4.022	4.37E+08	5.986
2	Al I	394.4	3.142	9.98E+07	
3	Ba II	455.4	2.722	4.44E+08	5.213
4	C I	247.8	7.68	8.40E+07	11.260
5	Ca I	422.6	2.932	6.54E+08	6.113
6	Ca II	396.8	3.123	2.80E+08	
7	Cu I	324.7	3.817	5.58E+08	7.726
8	C2 Swan	516.8[a]	–	–	–
9	CN UV	388.5[a]	–	–	–
10	Fe I	372.3	3.332	1.78E+08	7.902
11	Fe I	438.3	4.312	5.50E+08	
12	Fe II	259.9	4.768	2.35E+09	
13	H I	656.3	12.088	7.94E+08	13.598
14	K I	769.9	1.610	7.50E+07	4.341
15	Li I	670.8	1.848	1.48E+08	5.392
16	Mg I	285.2	4.345	1.47E+09	7.646
17	Mg II	279.6	4.433	1.04E+09	
18	Mn I	403.1	3.075	1.40E+08	7.434
19	Mn II	257.6	4.811	2.52E+09	
20	N I	746.8	11.996	7.84E+07	14.534
21	Na I	589.6	2.102	1.23E+08	5.139
22	O I triplet	777.2	10.741	2.58E+08[b]	13.618
23	Pb I	405.8	4.375	2.70E+08	7.417
24	Rb I	780.0	1.589	1.52E+08	4.177
25	Si I	288.1	5.082	6.51+E08	8.152
26	Ti II	308.8	4.061	1.20E+09	6.828
27	Ti II	334.9	3.749	2.2E+09	
28	Ti II	336.1	3.715	1.58E+09	

[a] Bandhead.
[b] The most intense transition.

Images of the substrate before and after placing the particles were acquired by a commercial HD camera mounted above the target at distance of about 80 mm. The area captured by the camera has dimensions

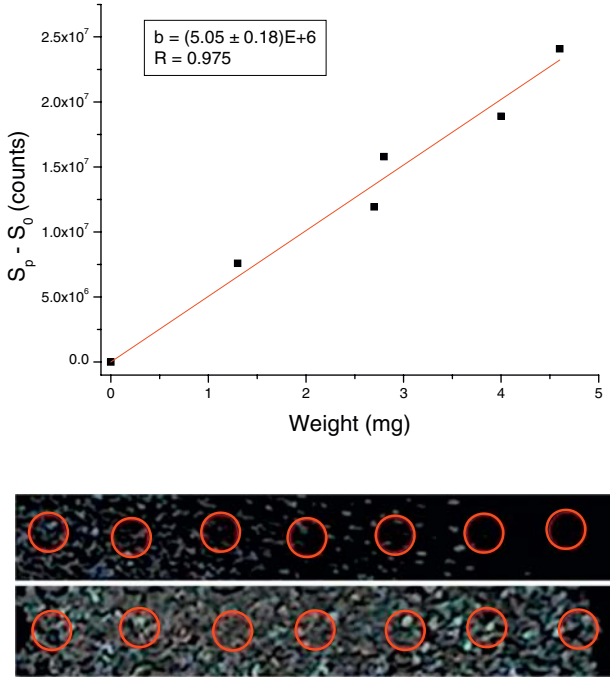

Fig. 2. Top – calibration for measuring particle weights; bottom - examples of the laser spots (red contours) along the lines with low (0.68–3.3 μg per spot) and high (6.4–8.7 μg per spot) particle loadings. The sample is ISE 992. (For interpretation of the references to colour in this figure legend, the reader is referred to the web version of this article.)

Table 4
Calibration coefficient b for retrieval of the sample weight from the photographs and the maximum particle loading for the linear dependency.

Sample	Colour	b (counts/mg) * 10^6	Max. loading (mg)
Al_2O_3	White	10.7 ± 0.38	3
NIST 2709	Light brown	6.36 ± 0.98	3.5
NIST2710	Light	14.4 ± 2.1	5
NIST 2711	Brown	4.18 ± 0.23	4
ISE 992	Light brown	5.05 ± 0.18	5
1632a	Black	5.84 ± 0.11	1.5
1633a	Dark grey	8.9 ± 1.2	3

of about 16 mm × 24 mm. The illumination conditions were fixed, provided by a white light source and two fiber bundles placed oppositely, at angle of about 50° with respect to the target plane.

For the image calibration, the substrate on the aluminum disk was weighted (A&D Instruments Ltd. Mod. HR-120-EC) before and after delivering the particles. Due to a poor scale resolution (±0.1 mg), weightings were done for sample masses much larger than in the LIBS measurements. This implies that the estimated weights inside the laser spot cannot be considered as absolute values.

All routines for the data processing were developed under LabVIEW environment, generating the reports with the filename, the spot position, the peak intensities and the signal-to-noise ratio (SNR) for all the selected lines, listed in Table 3.

3. Results and discussion

The chosen sample preparation method, consisting in particle attachments on a thin oil film over silica wafer, has an advantage of enhancing the plasma emission from sample. Moreover, high substrate purity ensures low interference with elements in samples; the used materials are cheap and could be disposed after the measurements. Here we applied a different method for the data acquisition with respect to [15–16,20], registering the single shot spectra instead of accumulating the signal. In this way, it was possible to monitor eventual line saturations in some hits and the spectral intensities for different particle loadings or distributions on the substrate. Monitoring intensities of the single shot spectra, here strongly variable from one laser spot to another also gives insight into the matrix effect and may indicate a strategy for its reduction.

3.1. Estimation of particle weights

Unlike a bare silica wafer, the same covered with the oil film is highly absorbing. The photographed substrate has the average pixel intensity $P_{av} < 0.2$ only on a scale 0–255, and this is favorable for observing the added particles. We performed the image calibrations by plotting the summed pixel intensity S_p over the substrate after subtracting the value S_0 measured before adding particles, versus the sample mass (Fig. 2– top). The retrieved linear coefficient b (counts/mg), specified in Table 4 for each sample, was then used to estimate the particle mass m (μg) inside a single laser spot as:

$$m(\mu g) = 10^{-3} * \frac{S_s - P_{av} * A_s}{b} \quad (1)$$

where S_s is a sum of the measured pixel intensities inside the laser spot, P_{av} is the average pixel intensity on blank (unloaded) support, and A_s is area of the laser spot in pixels. Contour of the laser spot was initially determined from repeated pictures of the laser induced craters on bare wafer, and then fixed for the further measurements. The laser spot area $\boldsymbol{A_s}$ here corresponds to 256 pixels.

The linear fit coefficient b differs up to a factor 3 from one sample to another, and it depends on particle size, not known for all the examined materials. The particle size determines the light scattering and consequently - the measured pixel intensities. A striking example of effect of the scattering on the pixel intensity is represented by samples ISE 992 and SRM 1632, which have very similar calibration coefficients *b* although the first material has a light colour and the latter is almost black. Colour of the bulk material (large quantity) influences the saturation point in the calibration graph. For the black sample SRM 1632 the saturation occurs already at weight of 1.5 mg. White Al_2O_3 powder also saturates for a relatively small particle mass because this material has low specific weight and, once spread over the substrate, it rapidly approaches aspect of the bulk. Since we were interested in estimating roughly the particle weights for small loadings, the image calibration was limited to the linear range, corresponding to the maximum particle mass specified in Table 4.

Fig. 2 – bottom shows details of pictures used to estimate the particle weights inside the laser spot (encircled by red) in case of the first sampled line - with low material loading, and the last line - with the maximum loading. For the reference material here (ISE 992) the estimated particle mass inside the laser spots varies between 0.5 μg and 11 μg, as specified in Table 5. These values are only the indicative because the calibration was performed for much higher mass loadings, but they are very useful for evaluating the differences among the sampling points. (For interpretation of the references to colour in this figure legend, the reader is referred to the web version of this article.)

3.2. LIBS spectra and indicators of the plasma parameters

In absence of particles the laser-substrate interaction is very weak and the spectra are dominated by CN and C_2 bands. These spectra also contain the Na I doublet, attributed to a presence of sodium in air, and weak C I (247.8 nm) and Si I (at 288 nm) lines. In presence of particles, even invisible by an eye, the emission lines both from the sample and the substrate become intense (Fig. 3). The plasma intensity depends not only on the estimated mass of particles, but also on their distribution inside the laser spot. A fully covered substrate approaches the case of bulk sample material, where we detected weaker lines than for a partial substrate's coverage (Fig. 4). This means that the chosen substrate enhances interaction between the laser and the sample. Indeed, we detected the most intense spectra on spots with relatively low particle loadings (see Table 5). Si I and C I lines are not well correlated with

Table 5
Range of the estimated particle weights inside the laser spot, of the ionic to atomic line ratios R(Mg), of peak ratios of CN and C line, and the sample mass inside the laser spot for which the maximum R(Mg) was detected.

Sample	Weight inside the laser spot (μg)	R(Mg)	WL H_α (nm)	$I_p(CN)/I_p(C)$	Weight (μg) for max. R(Mg)
NIST 2709	1.6–11.0	3.9–0.72	0.69–0.18	4.6–45.6	3.8
NIST 2710	0.54–9.2	11.8–1.4	0.98[a]–0.31	0.72–13.4	1.2
NIST 2711	0.77–7.2	7.6–2.9	0.92–0.62	1.7–2.8	1.9
ISE 992	0.68–8.7	3.2–0.64	0.56–0.29	1.8–23.8	2.3
SRM 1632a	1.8–7.8	1.9–0.73	0.32–0.18	8.6–25.5	4.3
SRM 1633b	1.8–3.4	3.3–0.75	0.90–0.22	1.7–19.6	2.7

[a] Max. measured excluding the saturated lines.

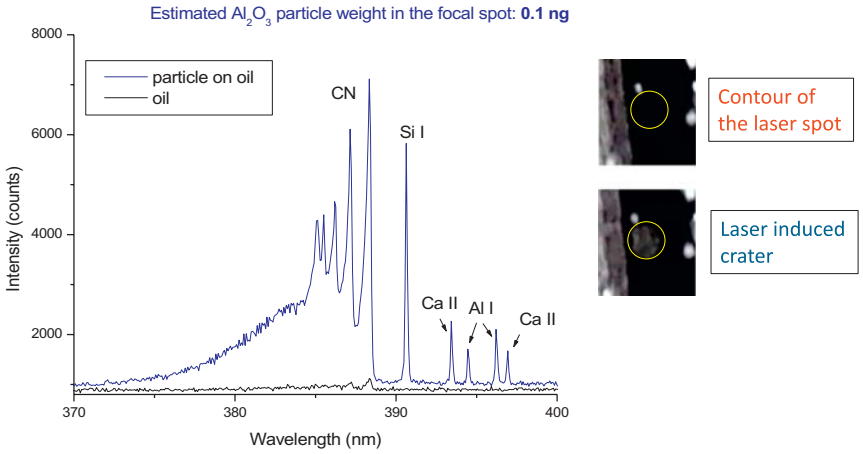

Fig. 3. Left – comparison between the spectrum from the bare substrate (black line) and the same with Al_2O_3 particles (blue line) with the estimated weight <0.1 ng inside the laser spot; right – photos of the substrate/sample before and after the laser pulse. (For interpretation of the references to colour in this figure legend, the reader is referred to the web version of this article.)

intensities of the lines belonging exclusively the sample. In such conditions we cannot measure Si and C content in particles as these elements represent interference from the substrate.

The acquired single-shot spectra were processed to retrieve the line peaks (Table 3) after subtracting the nearby background, eliminating those with signal-to-noise-ratio SNR < 3.5. The line peaks are extremely variable from one sampling point to another, ranging from the detection limit up to the detector's saturation in some cases. In particular, the sample NIST 2710 strongly interacts with the laser and about 30% of the acquired spectra present at least on saturated line among Hα, K I and Na I. The less intense spectra were detected on the coal SRM 1632 characterized by a large presence of carbon (>60%), the element which first ionization energy is very high (11.26 eV).

One of indicators of the plasma parameters is a ratio ionic/atomic line, both belonging to one element. Here we considered the Mg II and the Mg I lines from Table 3 because they are present in all the spectra, their wavelengths are close to each other and belong to the same spectrometer channel. We define their line intensity ratio as:

$$R(Mg) = \frac{I\,(Mg\ II)}{I(Mg\ I)} \qquad (2)$$

The measured R(Mg) shows large variations within the spectra from one sample, as summarized in Table 5. In the same table we also report the Lorentzian width (WL) of Hα line (determined from the line fitting by the Voigt profile), which is an indicator of the plasma electron density, then the peak ratio of the CN band-head and the C I line, as well as the estimated particle weight inside the laser spot for which R(Mg) has the maximum value. From Table 5 it could be observed that the lowest R(Mg), hence the plasma temperature, occurs on the coal NIST 1632. On the opposite, the samples NIST 2710 and NIST 2711 strongly interact with the laser and the measured R(Mg) is very high. The ratio CN/C is higher for lower values of R(Mg), indicating a cooler plasma dominated by molecular emission.

Fig. 5 shows an example of a single shot LIBS spectrum acquired on NIST 2711, where the estimated particle mass inside the laser spot was of 2.4 μg. Here it was possible to observe also the Cu I line well above the detection threshold, where this element has the certified concentration of 114 ppm. Furthermore, it is well known that the detection sensitivity could improve many times if summing the spectra that contain the specific signal above a certain threshold [12]. All these lead us to the conclusion that the chosen sample preparation allows to detect particle compositions with a high sensitivity. In order to estimate the analytical capability of the method we report in Table 6 the maximum SNR_{max} for different elements measured in the single shot spectra. Considering that the most intense spectra occur for intermediate sample masses inside the laser spot (Table 5) i.e. in presence of many particles, we might assume that the average element concentrations there

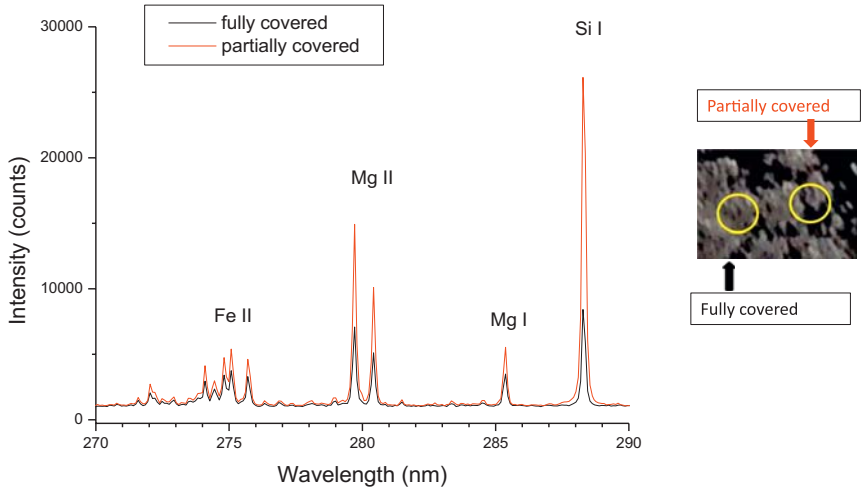

Fig. 4. Left – spectra from the ash particles NIST 1633 for a fully (black line) and a partially covered (red line) substrate; right - the corresponding photo of the sample with the laser spot contours. (For interpretation of the references to colour in this figure legend, the reader is referred to the web version of this article.)

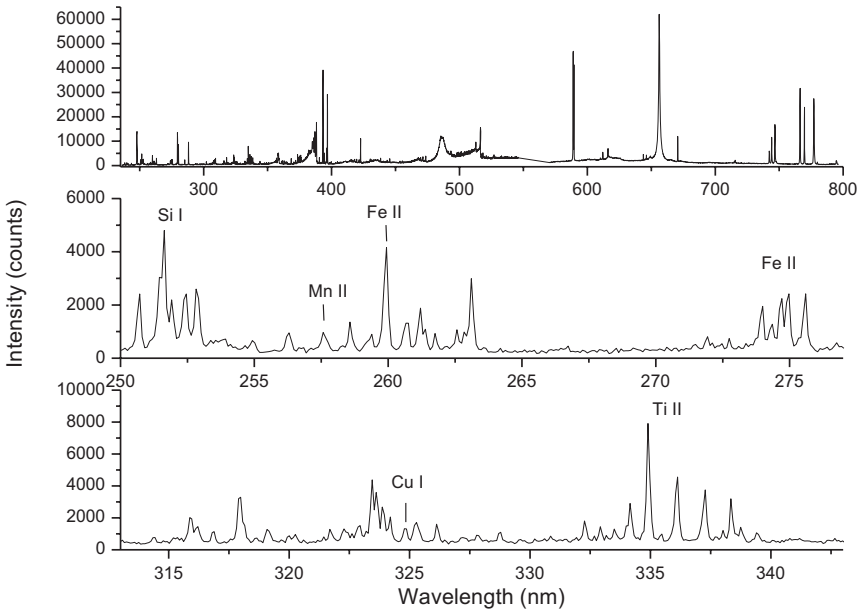

Fig. 5. Spectrum and its details for NIST 2711 particles with the estimated weight of 2.4 μg inside the laser spot.

correspond to the certified values. Here we achieved a single shot detection of Pb and Cu at concentrations of only 19 ppm and 35 ppm, respectively. On NIST 2710, characterized by a high plasma temperature and consequently - by a high ionization degree, SNR_{max} of the Pb I and the Cu I lines are lower than expected for relatively high concentrations of these elements in the sample.

3.3. Calibration for element quantifications

For a plasma in local thermal equilibrium (LTE) and neglecting reabsorption, the line intensity corresponding to atomic or ionic transition between levels E_k and E_i of the element Z is given by:

$$I^{ki}{}_Z = a'_{Z.} N_Z \frac{g_k A_{ki} e^{-E_k/kT}}{U_Z(T)} \equiv a'_Z N_Z f^{ki}_{1Z}(T) \quad (3)$$

where a'_Z is a constant depending on experimental conditions, g_k and A_{ki} are the level degeneracy and the tabulated transition probability, respectively, and U_Z (T) is the temperature dependent partition function of the considered species with density N_Z in the plasma.

In typical LIBS plasmas the species are present both in atomic and in first ionization state, and their relative concentration ratio in LTE conditions is given by the Saha's equation:

$$\frac{N_Z^+}{N_Z} = \frac{1}{N_e[cm^{-3}]} \cdot \frac{U_Z^+(T)}{U_Z(T)} B \cdot T[K]^{3/2} e^{-\frac{E_\infty}{kT}} \equiv f_{2Z}(N_e, T) \quad (4)$$

where: N_e is plasma electron density (cm^{-3}), $U_Z(T)$ and $U_Z^+(T)$ are partition functions of atoms and ions in the first ionization stage, respectively; E_∞ is the first ionization energy; k is the Boltzmann constant; B is a dimensionless constant with value of 4.825×10^{15}, which corresponds to $2 * (2\pi m_e k)^{3/2}/h^3$ and it has been calculated in [11] after appropriate unit conversions.

At an equivalent plasma excitation temperature, the percentage of atoms is larger at higher electron densities because of more efficient electron-ion recombination (Eq. (4)). At a fixed plasma electron density, the ionic emission increases with the excitation temperature; the same effect exists for the atomic species (Eq. (3)) but only up to a certain temperature where the thermal ionization suppresses further increase of

Table 6
The maximum signal-to-noise ratio (SNR_m) measured in single shot spectra from each sample, relative to the chosen analytical lines; the element concentrations in the samples are also specified.

Species[a]	λ (nm)	NIST 2709		NIST 2710		NIST 2711		ISE 992		SRM 1632		SRM 1633	
		SNR_m	Conc.	SNR_m	Conc.	SNR_m	Conc.	SNR_m	Conc.	SNR_m	Conc.	SNR_m	Conc.
Al I	394.4	187	7.50%	251	6.44%	419	6.53%	173	3.65%	162	2.95%	399	15.05%
Ba II	455.4	192	968 ppm	17	707 ppm	201	726 ppm	28	256 ppm	9	120 ppm	246	709 ppm
Ca II	396.8	812	1.89%	717	1.25%	1159	2.88%	534	2.94%	138	2410 ppm	801	1.51%
Cu I	324.8	66	34.6 ppm	13	2950 ppm	155	114 ppm	–	17.6 ppm	–	15.9 ppm	19	119 ppm
Fe I	372.3	97	3.50%	18	3.38%	73	2.89%	81	1.62%	51	1.11%	260	7.78%
Fe II	259.9	318		261		183		77		14		235	
K I	769.9	1137	2.03%	Sat.	2.11%	Sat.	2.45%	Sat.	1.43%	549	4110 ppm	919	1.95%
Li I	670.8	918	–	537	–	752	–	Sat.	25.9 ppm	248	39 ppm	973	–
Mg II	279.6	1561	1.51%	389	0.853%	985	1.05%	547	0.546%	29	1150 ppm	122	0.482%
Mn I	403.1	147	538 ppm	55	1.01%	54	638 ppm	26	244 ppm	–	29 ppm	7	131 ppm
Mn II	257.6	87		116		88		30		8		28	
Na I	589.6	942	1.16%	Sat.	1.14%	Sat.	1.14%	Sat.	6470 ppm	790	828 ppm	750	0.201%
Pb I	405.8	44	18.9 ppm	64	5532 ppm	64	1162 ppm	9	23.4 ppm	–	12.4 ppm	6	68 ppm
Rb I	780.0	34	–	41	–	130	–	397	68.5 ppm	9	30 ppm	26	140 ppm
Ti II	336.1	11	0.342%	89	0.283%	191	0.306%	59	2540 ppm	31	1750 ppm	194	0.791%

[a] Sat = saturated line on the detector.

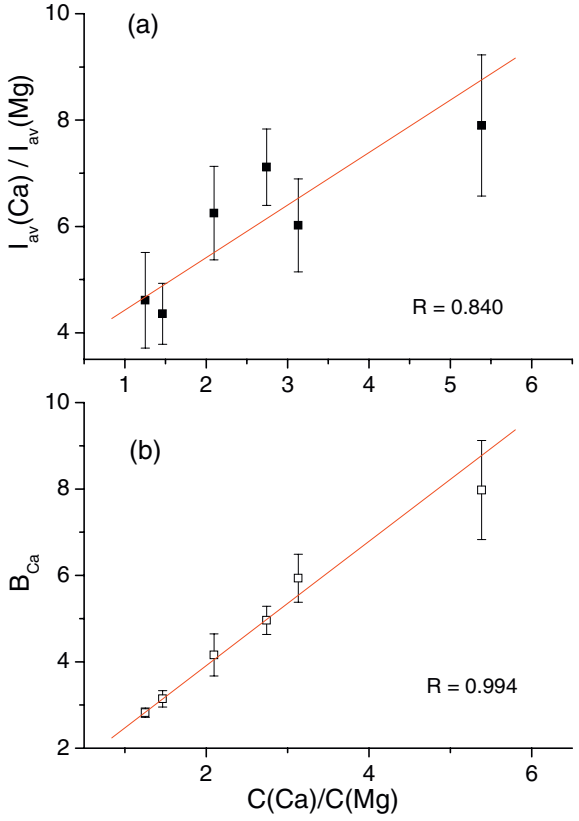

Fig. 6. Comparison between two calibration approaches for retrieval of the concentration ratio Ca/Mg: a) using the ratios of the average line intensities; b) using the linear growth coefficients B_Z retrieved from the single shot spectra.

the line intensities. Anyway, changes of the plasma parameters during LIBS measurements affect the line intensities both from the atomic and the ionic species.

In our recent work [11] we have shown that variations of the line intensities in LIBS plasmas are mainly caused by changes in the plasma temperature and less influenced by the electron density. In the present experiment, from the measured R(Mg) we might deduce that large variations of the plasma temperature exist inside a single data set (for one sample type). Furthermore, the spectra from the analyzed samples tend to group around very different plasma temperatures, and this is one of the reasons for so called matrix effect. Accordingly, in our LIBS measurements we might expect poorly correlated calibration curves, with large error bars, and this is exactly what occurs (Fig. 6 – top) where Ca I line at 422 nm was normalized to the chosen reference line (Mg I at 285 nm). For building up this calibrations graph, we considered 6 groups of the averaged spectra per sample: each group corresponds to seven spots in a raw with similar particle loadings, plus seven sparse samplings. It clearly appears that from the averaged spectra we cannot measure the relative element concentrations due to excessive variations of the plasma temperature across one sample - reflected in the large error bar, and from one sample to another – reflected in the point scattering.

In the common calibration approach it is assumed that the ratio of the average line intensities I^{av} is a function of the corresponding element concentrations C:

$$\frac{I_Z^{av}}{I_{REF}^{av}} = f\left(\frac{C_Z}{C_{REF}}\right) \tag{5}$$

where subscripts Z and REF are related to the measured and the reference element, respectively. We introduce the concentration ratio $C_{RZ} = C_Z / C_{REF}$. If the calibration graph is linear, we have:

$$\frac{I_Z^{av}}{I_{REF}^{av}} = a_Z + b_Z(C_{RZ}) \tag{6}$$

where b_Z and a_Z are constants for the chosen element transitions. Being usually $a_Z \approx 0$, the concentration measurements do not depend on the absolute line intensities but only on their ratio.

In presence of large intensity variations from one sampling point to another, as in our experiment, we propose not to consider the averaged

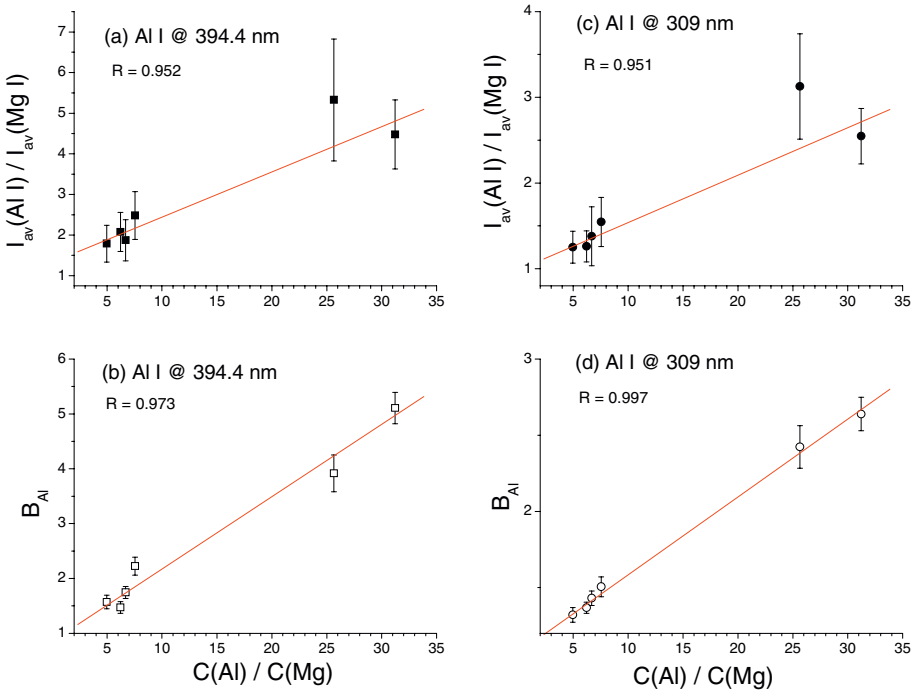

Fig. 7. Comparison between two calibration approaches for retrieval of the concentration ratio Al/Mg. Top - using the ratios of the average line intensities. Bottom – using the linear growth coefficients B_Z retrieved from the single shot spectra. The plots on the left (a, b) correspond to Al I line at 394.4 nm, on the right (c, d) they regard Al I transition at 309.3 nm.

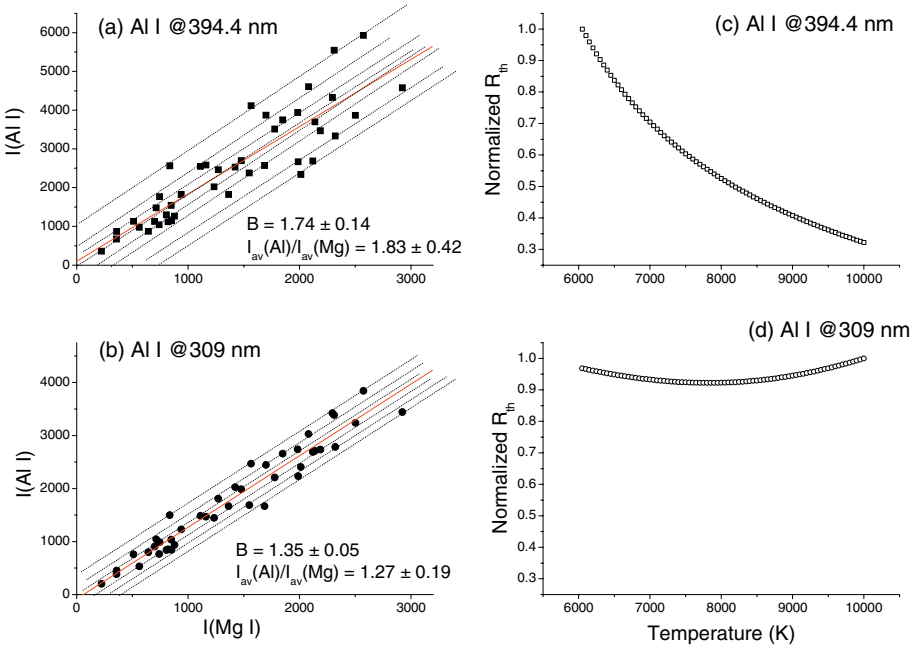

Fig. 8. Left panels - intensity of Al I line versus Mg I line for sample NIST 2709, where the linearly fitted growth is shown (red line). Right panels – the corresponding theoretical line intensity ratio (normalized) as a function of the plasma temperature. (For interpretation of the references to colour in this figure legend, the reader is referred to the web version of this article.)

spectra but to determine the linear fit coefficients $B_Z(C_{RZ})$ for each ensemble of single shot spectra corresponding to one sample:

$$I_Z = A_Z + B_z(C_{RZ}) \cdot I_{REF} \tag{7}$$

For all the examined cases the intercept is close to zero ($A_Z \approx 0$) although calculated with a large error. By comparing Eqs. (6) and (7) it is evident that the two linear coefficients intrinsically have similar values ($B_z \approx b_Z$). However, if the signal fluctuations are very large the error in calculating B_Z is much smaller than for the coefficient b (the line intensity ratio). Consequently, the calibrations performed by using the coefficients $B_Z(C_{RZ})$ instead of the line ratios produces much better results (Fig. 6 – bottom). Fig. 7 - top shows other examples of calibrations based on the averaged spectra, relative to two Al I transitions. Now, repeating the calibration but with the linear growth coefficients $B_z(C_{RZ})$, the precision and the linearity are importantly improved (Fig. 7 – bottom), particularly for the Al I transition at 309 nm.

Now, let's see in details how the calibration is outstandingly improved by considering the slopes B_Z of the analytical lines versus the reference line. In Fig. 8 - left panels, the peaks of Al I transitions at 309.3 and 394.4 nm, measured in single shot spectra, are plotted versus the Mg I line for the sample NIST 2709. The data points seem to align along parallel lines, here drawn arbitrary, where those on the left (with a larger intercept) generally correspond to a higher measured ratio R(Mg) i.e. to a higher plasma temperature. This indicates the real nature of large errors observed in calibrations by the averaged spectra (Figs. 6–7, top panels): the error bars here are equivalent to spreading of the intercepts, which depend on the plasma temperature. On the other hand, the slopes B_Z (red line in Fig. 8) also depend on the element concentration ratio but they are scarcely influenced by fluctuations of the plasma temperature among the spectra from one sample. Wider ranges of the line intensities inside the data sets allow calculating the slopes B_Z more precisely.

Much lower data spreading for Al I line at 309.3 nm than for the line at 394.4 nm (Fig. 8 – left panel) could be explained by simulations based on Eq. (2). The theoretical intensity ratio R_{th} of the analytical line I_Z and the reference line I_{REF} could be written as:

$$R_{th} = \frac{N_Z}{N_{REF}} \frac{f_{1Z}(T)}{f_{1REF}(T)} \tag{8}$$

where N_Z and N_{REF} are species concentration in plasma, $f_{1Z}(T)$ and $f_{1REF}(T)$ are the temperature dependent functions for the given transitions (see Eq. (2)):

$$f_1(T) = \frac{g_k A_{ki} e^{-E_k/kT}}{U(T)} \tag{9}$$

Approximation of the LTE usually holds for short integration periods, as for example, of a few microseconds. However, we believe that the spectra acquired with not gated detectors might also correspond to LTE conditions because, except for the atomic lines from very low excitation levels and the molecular transitions, the line intensities have approximately an exponential decay with short time constants. This means that the time integrated spectra are dominated by the line intensities present during the early plasma stage, where the LTE holds.

Table 7
Formulas for calculating the partition functions of different species, dependent on plasma temperature expressed in eV.

Species	Partition function
Mg I	$-0.68976 + 8.37684 * T_{ev} - 14.42823 * T_{ev}^2 + 9.1079 * T_{ev}^3$
Mg II	$2.19509 - 0.78372 * T_{ev} + 0.92923 * T_{ev}^2 - 0.26717 * T_{ev}^3$
Fe I	$19.79886 + 4.59506 * T_{ev} + 18.32766 * T_{ev}^2 + 33.74256 * T_{ev}^3$
Fe II	$26.6301 + 35.7434 * T_{ev} + 3.70962 * T_{ev}^2 + 10.40752 * T_{ev}^3$
Mn I	$5.7829 + 3.03974 * T_{ev} - 16.95296 * T_{ev}^2 + 30.51789 * T_{ev}^3$
Mn II	$7.94864 - 4.88212 * T_{ev} + 6.22598 * T_{ev}^2 + 9.684 * T_{ev}^3$
Al I	$4.27789 + 9.47982 * T_{ev} - 19.53664 * T_{ev}^2 + 14.23736 * T_{ev}^3$
Al II	$0.95935 + 0.24187 * T_{ev} - 0.53439 * T_{ev}^2 + 0.42161 * T_{ev}^3$
Ca I	$-4.37395 + 30.72767 * T_{ev} - 61.33914 * T_{ev}^2 + 45.54263 * T_{ev}^3$
Ca II	$2.13822 - 2.13253 * T_{ev} + 6.09014 * T_{ev}^2 - 1.97591 * T_{ev}^3$
Ti I	$23.59506 - 32.21196 * T_{ev} + 96.80733 * T_{ev}^2 + 24.16876 * T_{ev}^3$
Ti II	$26.27059 + 69.74564 * T_{ev} - 6.6582 * T_{ev}^2 + 3.58086 * T_{ev}^3$

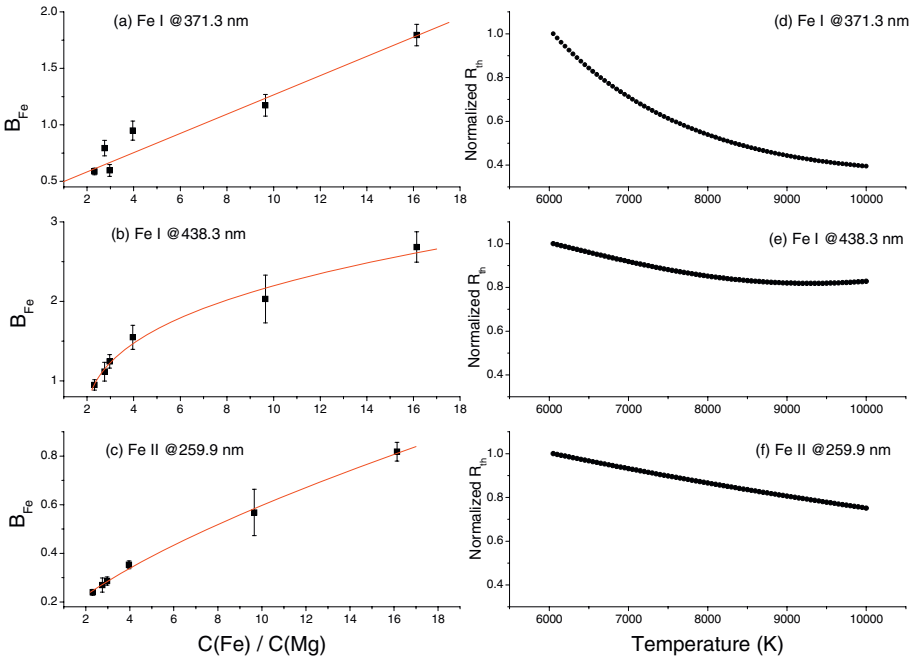

Fig. 9. Left panels - calibrations based on the slopes for two Fe I lines and one Fe II line. Right panels – the corresponding theoretical line intensity ratios (normalized) as a function of the plasma temperature.

Neglecting the temperature dependent changes in the ionization rate and assuming that N_Z and N_{REF} are proportional to the corresponding element concentrations in sample, from Eqs. (8)–(9) it is possible to evaluate the theoretical line intensity ratio R_{th}:

$$R_{th}(T) \sim \frac{C_Z}{C_{REF}} \cdot \frac{e^{-E_k^Z/kT}}{e^{-E_k^{REF}/kT}} \cdot \frac{U_{REF}(T)}{U_Z(T)} \quad (10)$$

Here we omitted the transition constants ($A_k g_k$) as they do not influence relative changes of R_{th} with the plasma temperature. This ratio depends on energy of upper transition levels of the selected lines and on the partition functions. In order to calculate R_{th} we retrieved from the NIST database values of the partition functions for different species in temperature range 0.5–1.05 eV (6000–12,000 K c.a.) with step of 0.025 eV. Partition functions of all here considered species could be very well approximated by 3rd order polynomials in the given temperature interval. Chi-square ranges between 0.9999 and 1.0 except for Al II (chi-square 0.998) because in this case U(T) changes very little (from 1.00 to 1.11) and the corresponding NIST data are given with two

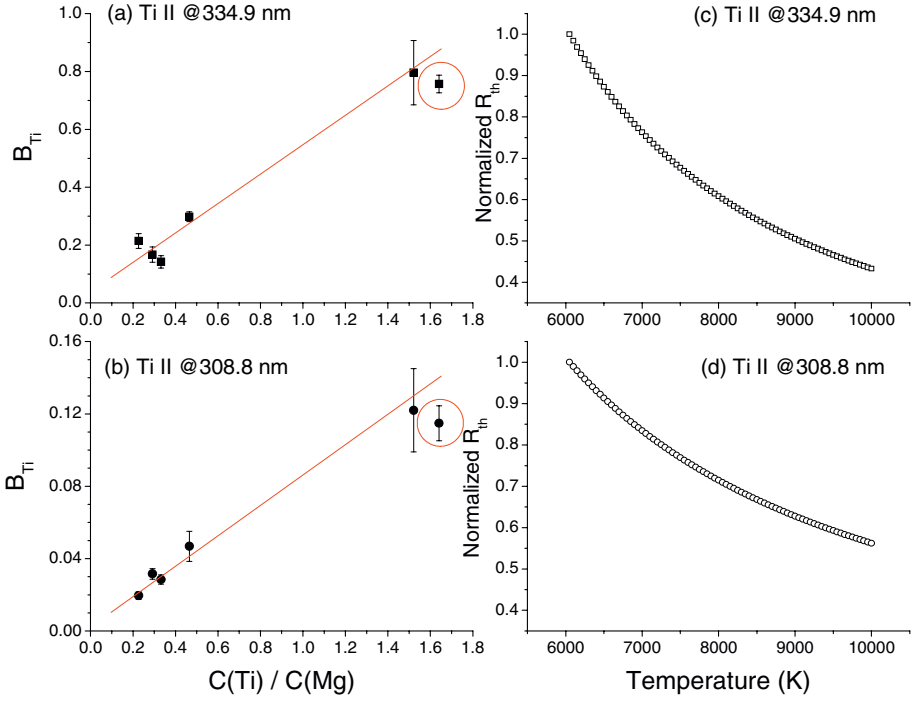

Fig. 10. Left panels - calibrations based on the slopes for two Ti II transitions. Right panels – the corresponding theoretical line intensity ratios (normalized) as a function of the plasma temperature. The point with the highest Ti/Mg concentration ratio was excluded from the fitting.

decimal digits only. The retrieved polynomial fit coefficients of the partition functions are reported in Table 7.

Fig. 8-right shows the normalized, theoretically calculated ratios Al I/Mg I as a function of the plasma temperature. The ratio involving Al I transition at 309.3 nm changes <8% in the whole temperature range here considered (6000 K–10,000 K), which is common for the LIBS plasmas in gases at atmospheric pressure. In case of Al I line at 394.4 nm, R_{th} rapidly decreases with the plasma temperature, changing for about 70% between 6000 K and 10,000 K. These dissimilarities in behavior of the line intensity ratios with the temperature explain the differences in data scattering among the single shot spectra (Fig. 8 – left) and on the calibration graphs (Fig. 7 – bottom) for the two examined Al I lines. When measuring the relative element concentrations it is of outmost importance to choose pairs of the element transitions that are weakly sensitive to variations of the plasma temperature. Such a choice improves the measurement precision and it is essential for reducing the matrix effect because dissimilar materials might interact differently with the laser, producing plasmas with very different average temperatures.

Fig. 9-left compares the calibration graphs for two Fe I lines and one Fe II transition; the corresponding R_{th} calculated for different plasma temperatures are shown on the figure's right. Atomic Fe transition at 371.3 nm produces the calibration graph with two points well above the linear fit. These points belong to NIST 2710 and 2711, on which the laser induced plasmas have high temperature with respect to the other samples. In fact, R_{th} for this line normalized on the Mg I transition changes for about 60% in the considered temperature range, and this explains the large data scattering in the calibration graph. The theoretical ratio of Fe I line at 438.3 nm and the Mg I line is much less sensitive to the temperature variations, so the points in the calibration plot are better aligned than in the previous case although the saturation occurs. For the relative concentration measurements C(Fe)/C(Mg) the best calibration was obtained for the ionic transitions (Fe II and Mg II), which ratio is also only weakly influenced by the plasma temperature. In this case the curve's growth is almost linear, the points are well aligned and the error bars are small except for the sample SRM 1632 where the large uncertainty is caused by low SNR of the Fe II line.

Other examples of the calibration graphs are shown in Fig. 10 and regard two Ti II transitions normalized to the Mg II line. In both cases the point corresponding to SRM 1633, with C(Ti) = 0.79% - more than twice higher in the other samples, was excluded from the linear fit. The theoretical line ratio involving Ti II transition at 308.8 nm is less sensitive to the temperature variations compared to Ti II line at 334.9 nm, so the corresponding calibration graph is less scattered. The large error bars for the samples SRM 1632 and ISE 992 are caused by low SNR of the Ti II line.

4. Conclusions

The substrate here employed for trapping particles prior to the LIBS measurements have the following advantages: both the oil and the wafer have high purities, low costs, and their emission lines in the plasma do not interfere importantly with spectra from the particles; the substrate itself interacts weakly with the laser, but it strongly enhances the plasma emission from the deposited sample material. The detection sensitivity is high, and in a single shot acquisition some trace elements were observed, like Pb in concentration below 20 ppm. The proposed sample preparation might become a good alternative to powder pressing into pellets (like soils) because the spectral emission is enhanced by the substrate and the sample consumption is very low.

The extreme fluctuations of line intensities among the spectra from one sample are caused both by variable particle weight and distribution inside the laser spots, as ascertained by on-line photography. Averaging the spectra prior to the calibration, even if plotting the line ratios versus the element concentration ratios, generates errors too large for evaluating the sample compositions. Intensities of an analytical and the reference line from single shot spectra are linearly correlated, the corresponding slope also depends on the relative element concentration but it is weakly influenced by fluctuations of the plasma temperature. Calibrations based on the line slopes instead of the line ratios reduced significantly the errors bars (from 20 to 50% to <10%), making possible to measure the sample compositions. In case of much smaller variations of the plasma intensities than here, as in sampling of flat homogeneous materials, the use of the slopes for the calibrations instead of the line intensity ratios should be still evaluated.

The matrix effect was evident from the scattered points on the calibration graphs because of very different mean plasma temperatures from one sample to another. In order to overcome this problem, we simulated theoretically the behavior of the line ratios with the plasma temperature. The line ratios depend both on the excitation levels of the transitions and on the temperature dependent partition functions of the species - here extrapolated by 3rd order polynomials. The proposed simulations are useful for selecting the line pairs less sensitive to changes of the plasma temperature, important both for improving the precision and for reducing the matrix effect. Knowing a-priori which spectral lines should be used for calibration also helps in setting-up the experiment in terms of the spectral detection range, and in establishing the data elaboration procedures – particularly important when dealing with large number of measurements and/or emission lines.

Acknowledgments

This work was supported by the FP7 Project EDEN, EC grant 313077.

References

[1] R. Fantoni, L. Caneve, F. Colao, L. Fornarini, V. Lazic, V. Spizzichino, Methodologies for laboratory laser induced breakdown spectroscopy semi-quantitative and quantitative analysis - a review, Spectrochim. Acta, Part B 63 (2008) 1097–1108.
[2] R.S. Harmon, R.E. Russo, R.R. Hark, Applications of laser-induced breakdown spectroscopy for geochemical and environmental analysis: a comprehensive review, Spectrochim. Acta B 87 (2013) 11–26.
[3] R.C. Wiens, S. Maurice, J. Lasue, O. Forni, R.B. Anderson, S. Clegg, S. Bender, D. Blaney, B.L. Barraclough, A. Cousin, L. Deflores, D. Delapp, M.D. Dyar, C. Fabre, O. Gasnault, N. Lanza, J. Mazoyer, N. Melikechi, P.-Y. Meslin, H. Newsom, A. Ollila, R. Perez, R.L. Tokar, D. Vaniman, Pre-flight calibration and initial data processing for the ChemCam laser-induced breakdown spectroscopy instrument on the Mars Science Laboratory rover, Spectrochim. Acta, Part B 82 (2013) 1–27.
[4] N.B. Zorov, A.A. Gorbatenko, T.A. Labutin, A.M. Popov, A review of normalization techniques in analytical atomic spectrometry with laser sampling: from single to multivariate correction, Spectrochim. Acta, Part B 65 (2010) 642–657.
[5] V. Lazic, A. Trujillo-Vazquez, H. Sobral, C. Márquez, A. Palucci, M. Ciaffi, M. Pistilli, Corrections for variable plasma parameters in laser induced breakdown spectroscopy: application on archeological samples, Spectrochim. Acta, Part B 122 (2016) 103–113.
[6] C. Chaleard, P. Mauchien, N. Andre, J. Uebbing, J.L. Lacour, C.J. Geertsen, Correction of matrix effects in quantitative elemental analysis with laser ablation optical emission spectrometry, J. Anal. At. Spectrom. 12 (1997) 183–188.
[7] U. Panne, C. Haisch, M. Clara, R. Niessner, Analysis of glass and glass melts during the vitrification process of fly and bottom ashes by laser-induced plasma spectroscopy. Part I: normalization and plasma diagnostics, Spectrochim. Acta Part B 53 (1998) 1957–1968.
[8] V. Lazic, R. Fantoni, F. Colao, A. Santagata, A. Morone, V. Spizzichino, Quantitative laser induced breakdown spectroscopy analysis of ancient marbles and corrections for the variability of plasma parameters and of ablation rate, J. Anal. At. Spectrom. 19 (2004) 429–436.
[9] A.P.M. Michel, Review: applications of single-shot laser-induced breakdown spectroscopy, Spectrochim. Acta, Part B 65 (2010) 185–191.
[10] J. Frydenvang, K.M. Kinch, S. Husted, M.B. Madsen, An optimized calibration procedure for determining elemental ratios using laser-induced breakdown spectroscopy, Anal. Chem. 85 (2013) 1492–1500.
[11] D.W. Hahn, Laser-induced breakdown spectroscopy for sizing and elemental analysis of discrete aerosol particles, Appl. Phys. Lett. 72 (1998) 2960–2962.
[12] V. Lazic, F. Colao, R. Fantoni, V. Spizzicchino, Laser-induced breakdown spectroscopy in water: improvement of the detection threshold by signal processing, Spectrochim. Acta, Part B 60 (2005) 1002–1013.
[13] V. Lazic, R. Barbini, F. Colao, R. Fantoni, A. Palucci, Self-absorption model in quantitative laser induced breakdown spectroscopy measurements on soils and sediments, Spectrochim. Acta, Part B 56 (2001) 807–820.
[14] M.A. Gondan, Y.B. Habibullah, U. Baig, L.E. Oloore, Direct spectral analysis of tea samples using 266 nm UV pulsed laser induced breakdown spectroscopy and cross validation of LIBS results with ICP-MS, Talanta 152 (2016) 341–352.

[15] S.I. Gornushkin, J.M. Anzano, B.W. Smith, J.D. Winefordner, Effective normalization technique for correction of matrix effects in laser-induced breakdown spectroscopy detection of magnesium in powdered samples, Appl. Spectrosc. 56 (2002) 433–436.
[16] J.M. Anzano, M.A. Villoria, A. Ruiz-Medina, R.J. Lasheras, Laser-induced breakdown spectroscopy for quantitative spectrochemical analysis of geological materials: effects of the matrix and simultaneous determination, Anal. Chim. Acta 575 (2006) 230–235.
[17] D.W. Hahn, J.E. Carranza, Assessment of the upper particle size limit for quantitative analysis of aerosol using laser-induced breakdown spectroscopy, Anal. Chem. 74 (2002) 5450–5454.
[18] J.-H. Kwak, G. Kim, Y.-J. Kim, K. Park, Determination of heavy metal distribution in PM10 during Asian dust and local pollution events using laser induced breakdown spectroscopy (LIBS), Aerosol Sci. Technol. 46 (2012) 1079–1089.
[19] R.E. Neuhauser, U. Panne, R. Niessner, Laser-induced plasma spectroscopy (LIPS): a versatile tool for monitoring heavy metal aerosols, Anal. Chim. Acta 392 (1999) 47–54.
[20] Y. Tian, H. Ching Cheung, R. Zheng, Q. Ma, Y. Chen, N. Delepine-Gilonc, J. Yu, Elemental analysis of powders with surface-assisted thin film laser-induced breakdown spectroscopy, Spectrochim. Acta, Part B 124 (2016) 16–24.